Kinetics of Graphene Formation on Rh(111) Investigated by *In Situ* Scanning Tunneling Microscopy

Guocai Dong[†,‡] and Joost W. M. Frenken[†,*]

[†]Kamerlingh Onnes Laboratory, Leiden University, P.O. Box 9504, 2300 RA Leiden, The Netherlands and [‡]JiangNan Graphene Research Institute, Xiangyun Road 6, Wujin, Changzhou, China

ABSTRACT *In situ* scanning tunneling microscopy observations of graphene formation on Rh(111) show that the moiré pattern between the lattices of the overlayer and substrate has a decisive influence on the growth. The process is modulated in the large unit cells of the moiré pattern. We distinguish two steps: the addition of a unit cell that introduces one or more new kinks and the addition of further unit cells that merely advance the position of an existing kink. Kink creation is the rate-limiting step, with kink creation at small-angle, concave corners in the graphene overlayer exhibiting the lower barrier.

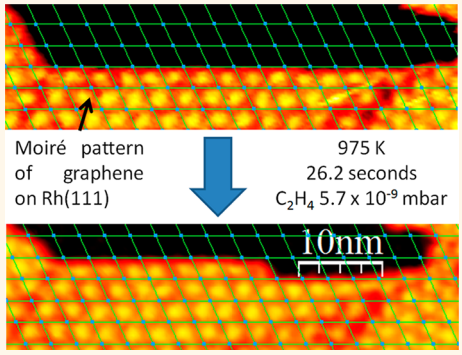

KEYWORDS: graphene · scanning tunneling microscopy · surface kinetics · chemical vapor deposition

Chemical vapor deposition (CVD) of hydrocarbons on metals provides a practical method for graphene production.[1−11] Insight into the basic steps of the growth process will prove essential for developing recipes for growing high-quality graphene.[8−13] In order to acquire such insight, direct observations at the elevated process temperatures would be very helpful. On the basis of more traditional measurements after cool-down, it is difficult to reconstruct the processes that have taken place at high temperature. However, it is technically challenging to perform atomic-scale observations at high temperatures, and because of this difficulty, only a few reports of this type exist. Using low-energy electron microscopy[9−11] and scanning electron microscopy,[14] several groups have performed *in situ* investigations of graphene growth from various sources, such as CVD, sublimation, or segregation on Ru and Ir. One of the important conclusions is that graphene growth is fed by the supersaturated, two-dimensional gas of C adatoms rather than by direct exchange between the C dissolved in the substrate and the graphene.[11] The advancement rate v of a graphene edge scales nonlinearly with the concentration of C adatoms S on the metal surface according to

$$v \propto \left[\left(\frac{S}{S^{eq}}\right)^{n} - 1\right] \qquad (1)$$

where $n = 5$ and S^{eq} is the equilibrium density of C with respect to the graphene islands.[10] The edge rate equals $v = (1/L)\mathrm{d}A/\mathrm{d}t$, where A and L are the area and perimeter of a graphene island. The temperature-independent value of 5 for n was interpreted as an indication that five C atoms are needed to form a cluster before they can be incorporated into the graphene structure.

In this article, we use high-temperature scanning tunneling microscopy (STM) movies to reveal the microscopic details of the growth kinetics of graphene on Rh(111). Clear evidence will be provided that on this surface the growth is modulated in unit cells of the moiré pattern between the overlayer and the substrate, which are much larger than a 5 atom C cluster. The entire STM movie used in this paper can be found online.[2] Here, we report images and quantitative data extracted from a single movie but note that we have repeated the procedure several times, each time with fully equivalent results.

* Address correspondence to frenken@physics.leidenuniv.nl.

Received for review May 4, 2013 and accepted July 7, 2013.

Published online July 07, 2013
10.1021/nn402229t

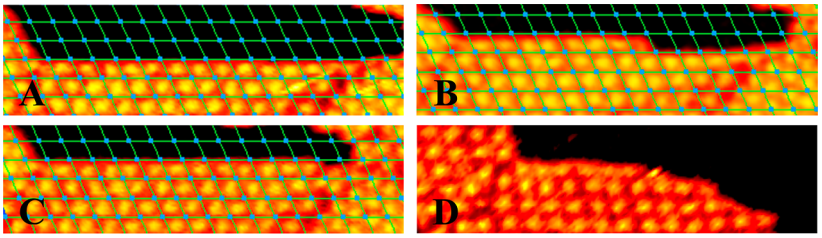

Figure 1. Four snapshots from an STM movie,[2] during graphene growth at 975 K on graphene-seeded Rh(111) at an ethylene pressure of 5.7×10^{-9} mbar. (A−C) Consecutive images (26.2 s each) of a graphene edge, starting out straight in (A), showing a kink in (B), which has advanced to the right in (C); all changes are discretized in units of the moiré pattern. (D) Incomplete moiré unit, as we observed occasionally. The grids in the image indicate the moiré pattern between graphene and the substrate. Image size: 55×15 nm^2. Sample voltage: −1.84 V. Tunneling current: 50 pA.

RESULTS AND DISCUSSION

Figure 1A−C shows three consecutive STM images. The structure that is clearly visible is the 2.9 nm moiré pattern between the aligned lattices of the graphene and the Rh. What is demonstrated by Figure 1 and is observed throughout the entire movie is that the advancement of the edges appears to proceed stepwise, in units of this moiré lattice. Entire rows of such units are added. Also within the rows the growth appears to proceed in moiré units. It starts along an edge by the creation of a new kink (or kink pair), which has a width of the period of the moiré lattice. After this, the new kink rapidly progresses along the edge, moving by single or multiple moiré units from image to image. This growth in moiré lattice units (288 C atoms when the graphene lattice is aligned with the Rh lattice) is reminiscent of the growth of hexagonal boron nitride on Rh(111).[15] The rate-limiting step in the formation of a single moiré unit most probably does not involve the simultaneous arrival of 288 atoms. Otherwise, the growth rate should be exceptionally nonlinear with respect to the ethylene pressure, which is in conflict with our observations and with the $n = 5$ of ref 10. This contradiction is resolved by a growth scenario, in which C edge adatoms first need to form a cluster of a certain critical size (*e.g.*, 5), after which the remainder of the moiré unit is formed rapidly. If this is indeed the case, it should be possible to observe intermediate configurations with incomplete moiré lattice units. Indeed, such configurations were observed, as is illustrated by Figure 1D. Recent theoretical work[16] predicted that the lattice mismatch between graphene and the metal substrate influences the growth of graphene, which is now confirmed by this observation. In energy terms, this implies that the energy landscape is modulated by the moiré structure: the lowest free-energy configuration is that of an integer number of moiré units, and the maximum free-energy configuration is one in which a small number of atoms is added to that. Further addition of atoms lowers the free energy until completion of the next moiré unit, and the free energy is at a minimum again. The growth is then modulated in large moiré units, but the critical nucleus is microscopic. The microscopic stable size can be 5 C atoms,[10] 24 C atoms (7 C_6 rings) as suggested by Wang *et al.*,[17] or as an increasing function of temperature,[18] and it can be different at various growth sites, such as straight edges or corners, as discussed below. In this scenario, eq 1 is still satisfied.

We analyzed two episodes from the STM movie, during which the ethylene pressure was 5.7×10^{-9} mbar. Figure 2 shows the images at the start and end of both episodes. Between panels A and B, the average edge advancement rates $|dA/Ldt|$ of the four graphene islands and the one graphene vacancy island (labeled 1−5) were determined to be 1.9 ± 0.7, 0.2 ± 0.3, 1.7 ± 1.5, 3.2 ± 0.5, and 49 ± 27 pm/s, respectively. In spite of the large error margins, we can draw two conclusions. First, island 2 grew at a much lower rate than the others. In fact, the size of island 2 remained unchanged during the entire 865 s period that it was in view of the STM. Second, the edge of the vacancy island (labeled 5) advanced much more rapidly (more than 20 times) than the rest. As these have been truly simultaneous observations, with all island and vacancy structures exposed to equal ethylene fluxes, we assume that the C adatoms' density near their edges should have been nearly equal. Therefore, we have to ascribe the differences in growth rate to differences in the edge configurations. The most important geometrical difference between graphene islands and vacancy islands is that the contour of a vacancy island naturally contains concave corners (*i.e.*, with angles below 180°), which can be of decisive importance. Adding the first new moiré unit requires the introduction of two new kinks along a straight step section, whereas it only requires a single kink at a concave corner. If we assume that the kink formation rate determines the rate at which new rows of moiré unit cells are initiated, this rate should be significantly higher at concave corners than at straight steps or convex corners. This point will be quantitatively confirmed in this article. To understand why small graphene islands, such as island 2, grow even more slowly, we assume that all graphene edges are populated by the same density S^{edge} of mobile C edge adatoms, in equilibrium with the C adatom density S on the surrounding metal substrate. The start of a new moiré unit cell requires the simultaneous presence of

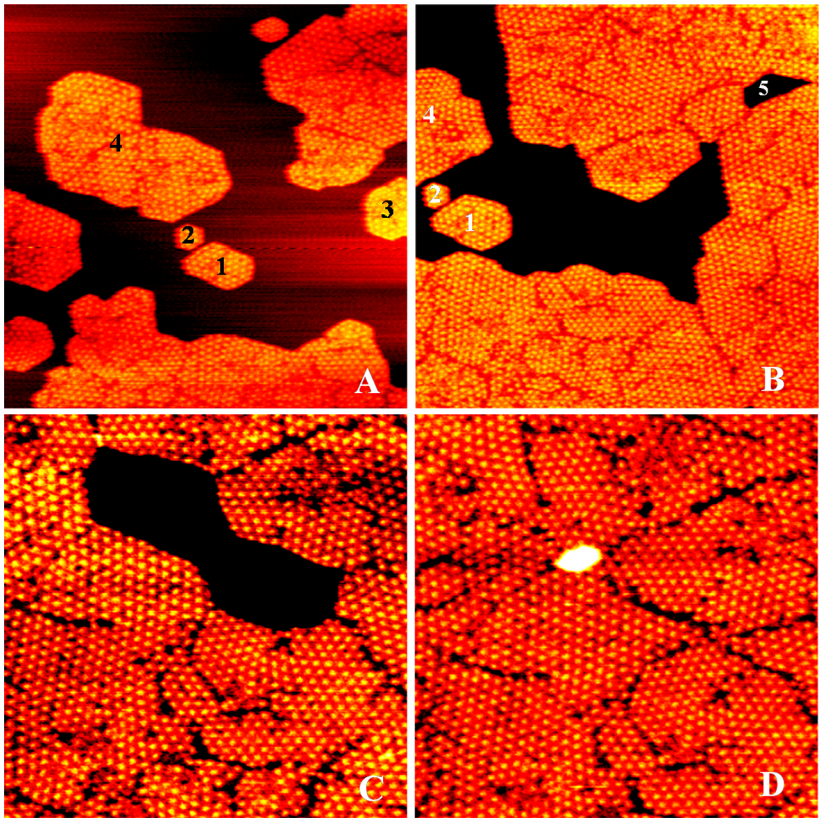

Figure 2. Four snapshots from the same STM movie as in Figure 1. Frame to frame analysis was performed for the 865 s period between panels A and B and the 524 s period between C and D. Sample voltage: −1.84 V. Tunneling current: 50 pA. Image sizes: 160 × 160 nm^2 for A and B; 100 × 100 nm^2 for C and D.

m C atoms, where *m* could be equal to the number $n = 5$, mentioned above. When the edge of the island is significantly shorter than am/S^{edge}, where *a* is the lattice constant of the graphene, the average number of C adatoms on the island edge is insufficient to get the process started, which leads to a significant suppression of the growth rate for the smaller islands. By contrast, the step advancement rate should be independent of size for the large graphene islands, as seems consistent with other work.[10]

In order to quantify the growth, we separate the process into two stages: kink creation and kink advancement, as shown in Figure 3A. The former introduces one or more new kinks, and the latter merely advances the position of an existing kink. Here we discuss direct measurements of the rates of kink formation, both on edges and at corners of the graphene and the rate of kink advancement. On internal edges of graphene vacancy islands, the creation and advancement of kinks was readily observed using STM, as shown in Figure 1. On external edges of graphene patches, we have hardly observed any kink; in most cases, we could only observe the sudden addition of a complete row with the width of the moiré lattice. So, we derive the advancement rate from internal edges and use the row addition rate to get the kink formation rate. We restrict the analysis of kink formation at corners and of kink advancement to a single vacancy island and to a limited time window, during constant ethylene pressure deposition, within which the change in geometry and the change in bulk C contribution (segregation) and CVD C contribution (deposition) could be very modest, which should result in a negligible variation in C adatom density on the metal surface. The advancement rate of a kink was measured to be 1230 C atoms per image (26.2 s acquisition time per frame) with a surprisingly high standard deviation of 580 C atoms. If the kink were to advance by uncorrelated single-atom events, the standard deviation should have been $(1230)^{1/2} = 35$. The strong statistical variation indicates that the growth proceeds in units much larger than a single C atom, namely, in units that are as large as $(580/35)^2 = 270$ atoms, fully consistent with a growth unit of 1 moiré unit cell (288 atoms). This indicates that graphene growth proceeds by the advancement of kinks that not only have a width of one complete moiré unit but also advance effectively in steps of single moiré units.

The creation rate of new kinks at corners was found to depend on the corner angle, as shown in Figure 3B. The maximum of 2 kinks/frame was still lower than the kink advancement rate of 4.3 moiré units/frame. The kink creation rate measured at the same ethylene pressure at straight edges was dramatically lower,

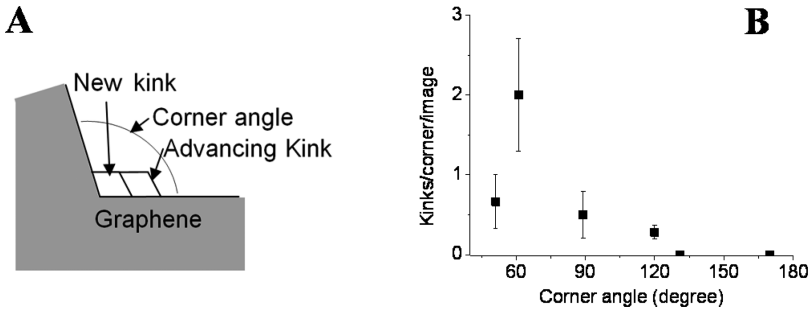

Figure 3. (A) Sketch of kink creation at a concave graphene corner and subsequent kink advancement. The nucleation and growth units correspond to complete unit cells of the moiré pattern. Note that a new kink introduces two extra corners (one concave and one convex), whereas the advancement does not require the creation of further corners. (B) Measured average number of kink creation events per STM image as a function of the angle of the concave graphene corner.

namely, 1.4×10^{-4} units/site/frame. Most kink creation events on straight edges were observed to take place at domain boundaries. We conclude that the creation of new kinks is the rate-limiting step, and that this is easiest at concave corners. Even though this conclusion of growth by kink formation and advancement consistent with previous work,[8−10] we should bear in mind that the kinks in the moiré pattern, discussed here, are much larger than the single graphene unit cell kinks considered before.

The dependence of the kink creation rate on corner angle in Figure 3B was counted from the kink creation events recorded for each of six selected corners. The error margins reflect the limited number in a total of 27 kink creation events that were counted. Figure 3B shows that it is very difficult to create a kink at a corner with an opening angle larger than 120°, and it suggests that there is a significant preference for kink formation at a 60° corner, which is a natural angle for the lattice of the graphene and that of the moiré pattern.

The fact that the growth of graphene takes place at kinks in the moiré pattern should be reflected in the statistical variations in the filling rate of graphene vacancy islands. This idea is tested in Figure 4B, where we have plotted the time dependence of the difference in vacancy island area between subsequent frames (episode between panels C,D in Figure 2). Figure 4B shows that the variations of the filling rate of the vacancy island are significant, beyond the inaccuracies in the STM measurement. For example, in the first 250 s in Figure 4B, the average filling rate is N = 1910 C atoms per frame, with a standard deviation of ΔN^{exp} = 1360 C atoms. The experimental inaccuracy on N is no more than ΔN^{error} = 510 C atoms. The extra variation $\Delta N = ((\Delta N^{exp})^2 - (\Delta N^{error})^2)^{1/2}$ amounts to 1260 C atoms, which is a factor of 29 larger than the expected number of $\sqrt{N}$, deriving from atom-by-atom statistics. This appears to support the notion that the effective growth unit is significantly larger than a single atom. However, assuming graphene to grow by building blocks of B C atoms, the statistical fluctuation is $\Delta N/N = 1/(N/B)^{1/2}$, which gives an estimate of B = 840 C atoms. This number is not only much larger than the 5 atom unit of ref 10 but also larger than the 288 C atom size of the moiré unit of graphene on Rh(111). We can easily understand this by realizing that growth only takes place at kink sites, the number of which K is also subject to statistical variations. The number of atoms added between subsequent images can be expressed, $N = RtK$, where R is the rate of C atoms attaching to each kink, t is the time between images, and K is the average number of kinks within the vacancy island. The combined effect on the fluctuation of N is expressed by $\Delta N = ((Rt\Delta K)^2 + (\Delta(Rt)\sqrt{K})^2)^{1/2}$. The first term in the square root derives from the fluctuations in the number of kinks, while the second represents the combination of the independent fluctuations in the advancement of K kinks. Both from individual images and from the ratio between the filling rate and the observed advancement rate of single kinks, we derive the same average number of kinks in the vacancy island of K = 1.6. Substituting this together with the measured values for Rt and $\Delta(Rt)$, we obtain an expected value for this fluctuation of 1700, which agrees reasonably well with the measured value of ΔN = 1260. Note that the main contribution to the statistical fluctuations in the filling rate results from the variation in the number of kinks.

Here we have concentrated on graphene regions that were aligned relatively well with respect to the Rh(111). The orientation and period of the moiré pattern depends sensitively on the relative orientation of the graphene and the substrate. Also, the energetic preference for forming complete moiré unit cells should be expected to depend significantly on the orientation. These aspects may influence the growth in a very complex way. Further experiments and theory are required to explore this in detail.

Since the edge growth speeds were so different for graphene islands and vacancy islands in Figure 2A,B, one may ask whether the edges were fed from the same source of C. As ethylene molecules only decompose on the bare metal surface,[7,9] the C supply should become lower while the graphene coverage increases. In order to understand this, we first consider the assumption that in a graphene vacancy C adatoms

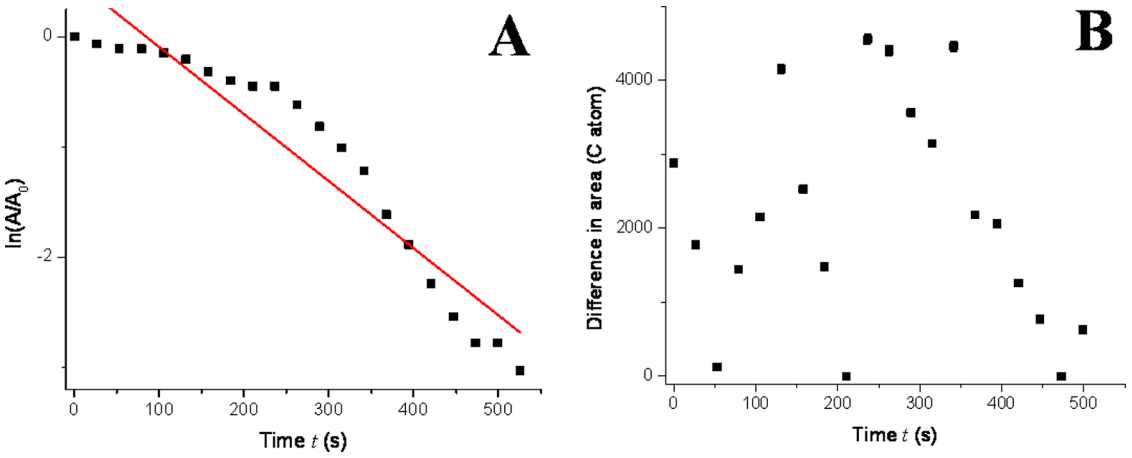

Figure 4. (A) Semilogarithmic plot of the time dependence of the area *A* of the enclosed Rh region in the episode between images C and D of Figure 2. The linear fit to the logarithm of the area has a slope of -6.1×10^{-3} s^{-1}. (B) Difference in area between subsequent frames for the same episode. The error derived from atom-by-atom statistic margins is within the symbol size.

cannot diffuse out of the enclosed Rh areas and the fraction of C escaping into the Rh substrate is negligible. Then, the total flux F of C atoms deposited on an enclosed Rh region should be proportional to the area A of this region, the impingement rate I of ethylene molecules, and the average number λ of C atoms deposited per impinging ethylene molecule. We equate the flux of deposited to the rate at which the Rh area fills up with graphene:

$$\frac{dA}{dt} = -\frac{A}{D} I\lambda = -\frac{A}{D}\lambda \frac{P}{\sqrt{2\pi m k_B T}} = -\alpha A P \lambda$$

where D is the areal density of C atoms in the graphene overlayer and I is expressed in terms of the ethylene pressure P, the (gas) temperature T, and the mass m of ethylene, using kinetic gas theory. The part that has remained unchanged during deposition has been combined in the constant α, which equals 7.5×10^4 mbar^{-1} s^{-1} for ethylene gas at 293 K. Based on this equation, we expect exponential decay of the uncovered area:

$$\ln\left(\frac{A}{A_0}\right) = -\alpha P \lambda t \qquad (2)$$

We have tested this in Figure 4A by plotting the time dependence of the measured area of the enclosed Rh regions during the episode between Figure 2C,D on a semilogarithmic scale. From the slope of the straight-line fit in Figure 4A, of -6.1×10^{-3} s^{-1}, and the ethylene pressures, we obtain an average value of $\lambda = 14$. This λ value suggests that each ethylene molecule was accompanied by the addition of an average of 14 C atoms to the growing graphene layer. This greatly exceeds the two C atoms in an ethylene molecule. Several sources of systematic error may have influenced the value of λ determined here. For example, the difference in position between the pressure gauge and the sample may have led to a systematic over- or underestimate of the local pressure at the Rh substrate. Similarly, the presence of the STM tip may have reduced the ethylene pressure locally, precisely in the field of view of the STM. Whereas the tip effect could only *reduce* the apparent λ, the geometry of our UHV system is such that the first effect cannot lead to an apparent *increase* of λ by more than a factor 2. The data points in Figure 4A can also be divided into more than one linear region. For instance, the first one starts from $t = 0$ to $t = 250$ and the second starts from $t = 250$ onward. Then λ values of 5.6 and 21 can be drawn from the linear fits, which are still larger than 2. Therefore, we are forced to conclude that the extra C atoms must have come from the C that was dissolved in the Rh substrate during earlier stages of the deposition. The segregation of dissolved C adds a memory effect to the effective flux of C to the surface. In the early stages of graphene growth, the adatom density is high, causing by the low growth speed of graphene discussed above, resulting in a high rate of C dissolution. By contrast, the final stages (*e.g.*, when the vacancy islands in the graphene are filling up) are characterized by much shorter adatom residence times and, hence, much lower adatom densities. During these stages, the dissolved C will partly resurface and contribute to the growth rate of the graphene. We suggest that this effect is causing the high λ value derived above. Although graphene formation by segregated C is well-known to occur during cool-down of C-exposed metals, here the supply of C to the surface *via* segregation from the bulk was active under the same conditions as the direct supply from the ethylene gas phase. The factor determining whether dissolution or segregation dominated was the local graphene geometry, namely, dissolution for isolated graphene patches *versus* segregation for vacancy islands in the graphene.

CONCLUSIONS

In conclusion, we have shown that the moiré pattern plays an important role in the growth of graphene on

Rh(111). Graphene has a preference to form complete moiré unit cells, which modulates the growth. After reaching the critical nucleus for the addition of one moiré unit, which we speculate to be a small number of added C atoms, the remaining atoms follow to quickly complete the rest of the moiré unit. By direct measurements of the adding rates of moiré units at different sites, we have drawn the following conclusions. Growth proceeds by kink creation and kink advancement, with kink creation being the rate-limiting step. After a kink unit has been created on the edge of graphene, a full row of new moiré units quickly follows one by one. It is easier to create a kink at concave corners of graphene. For this reason, the average growth rate in vacancy islands is much higher than that of compact islands. Because kink creation is the limiting step for graphene growth, differences in kink creation barrier also result in different C adatom densities during graphene growth, which has an effect on the flux of C dissolving into or segregating out of the Rh substrate.

METHODS

All measurements were performed in an ultrahigh vacuum system with a variable-temperature STM.[19,20] Temperatures were measured by a K-type thermocouple, spot-welded on the sample. Gas pressures were measured by an ionization gauge, accounting for the sensitivity for ethylene. The clean Rh(111) surface[21] was exposed to 1.3×10^{-5} mbar of ethylene at 293 K and heated to 975 K to form graphene islands. On this graphene-seeded surface, which was held at 975 K throughout the rest of the experiment, STM images were recorded continuously over a period of 76 min, while it was exposed to ethylene at pressures increasing from 1.3×10^{-10} to 1.5×10^{-8} mbar. For this paper, we have analyzed selected episodes from the STM movie, during which the ethylene pressure was at a constant value of 5.7×10^{-9} mbar.

Conflict of Interest: The authors declare no competing financial interest.

Acknowledgment. This research was supported by the Dutch Science Foundation NWO/FOM and by an ERC Advanced Investigator Grant.

REFERENCES AND NOTES

1. Coraux, J.; N'Diaye, A. T.; Busse, C.; Michely, T. Structural Coherency of Graphene on Ir(111). *Nano Lett.* **2008**, *8*, 565–570.
2. Dong, G. C.; van Baarle, D. W.; Rost, M. J.; Frenken, J. W. M. Graphene Formation on Metal Surfaces Investigated by *In-Situ* Scanning Tunneling Microscopy. *New J. Phys.* **2012**, *14*, 053033.
3. Kim, K. S.; Zhao, Y.; Jang, H.; Lee, S. Y.; Kim, J. M.; Kim, K. S.; Ahn, J. H.; Kim, P.; Choi, J. Y.; Hong, B. H. Large-Scale Pattern Growth of Graphene Films for Stretchable Transparent Electrodes. *Nature* **2009**, *457*, 706–710.
4. Martoccia, D.; Willmott, P. R.; Brugger, T.; Bjorck, M.; Gunther, S.; Schleputz, C. M.; Cervellino, A.; Pauli, S. A.; Patterson, B. D.; Marchini, S.; *et al.* Graphene on Ru(0001): A 25×25 Supercell. *Phys. Rev. Lett.* **2008**, *101*, 126102.
5. Oshima, C.; Tanaka, N.; Itoh, A.; Rokuta, E.; Yamashita, K.; Sakurai, T. A Heteroepitaxial Multi-Atomic-Layer System of Graphene and H-Bn. *Surf. Rev. Lett.* **2000**, *7*, 521–525.
6. Sutter, P. Epitaxial Graphene How Silicon Leaves the Scene. *Nat. Mater.* **2009**, *8*, 171–172.
7. Wintterlin, J.; Bocquet, M. L. Graphene on Metal Surfaces. *Surf. Sci.* **2009**, *603*, 1841–1852.
8. Luo, Z.; Kim, S.; Kawamoto, N.; Rappe, A. M.; Johnson, A. T. C. Growth Mechanism of Hexagonal-Shape Graphene Flakes with Zigzag Edges. *ACS Nano* **2011**, *5*, 9154–9160.
9. Loginova, E.; Bartelt, N. C.; Feibelman, P. J.; McCarty, K. F. Factors Influencing Graphene Growth on Metal Surfaces. *New J. Phys.* **2009**, *11*, 063046.
10. Loginova, E.; Bartelt, N. C.; Feibelman, P. J.; McCarty, K. F. Evidence for Graphene Growth by C Cluster Attachment. *New J. Phys.* **2008**, *10*, 093026.
11. McCarty, K. F.; Feibelman, P. J.; Loginova, E.; Bartelt, N. C. Kinetics and Thermodynamics of Carbon Segregation and Graphene Growth on Ru(0001). *Carbon* **2009**, *47*, 1806–1813.
12. Saadi, S.; Abild-Pedersen, F.; Helveg, S.; Sehested, J.; Hinnemann, B.; Appel, C. C.; Nørskov, J. K. On the Role of Metal Step-Edges in Graphene Growth. *J. Phys. Chem. C* **2010**, *114*, 11221–11227.
13. Rut'kov, E. V.; Gall, N. R. Role of Edge Atoms of Graphene Islands on Metals in Nucleation, Growth, Alkali Metal Intercalation. *Phys. Solid State* **2009**, *51*, 1738–1743.
14. Sutter, P. W.; Flege, J. I.; Sutter, E. A. Epitaxial Graphene on Ruthenium. *Nat. Mater.* **2008**, *7*, 406–411.
15. Dong, G. C.; Fourre, E. B.; Tabak, F. C.; Frenken, J. W. M. How Boron Nitride Forms a Regular Nanomesh on Rh(111). *Phys. Rev. Lett.* **2010**, *104*, 096102.
16. Wu, P.; Jiang, H. J.; Zhang, W. H.; Li, Z. Y.; Hou, Z. H.; Yang, J. L. Lattice Mismatch Induced Nonlinear Growth of Graphene. *J. Am. Chem. Soc.* **2012**, *134*, 6045–6051.
17. Wang, B.; Ma, X.; Caffio, M.; Schaub, R.; Li, W.-X. Size-Selective Carbon Nanoclusters as Precursors to the Growth of Epitaxial Graphene. *Nano Lett.* **2011**, *11*, 424–430.
18. Zangwill, A.; Vvedensky, D. D. Novel Growth Mechanism of Epitaxial Graphene on Metals. *Nano Lett.* **2011**, *11*, 2092–2095.
19. Hoogeman, M. S.; van Loon, D. G.; Loos, R. W. M.; Ficke, H. G.; de Haas, E.; van der Linden, J. J.; Zeijlemaker, H.; Kuipers, L.; Chang, M. F.; Klik, M. A. J.; *et al.* Design and Performance of a Programmable-Temperature Scanning Tunneling Microscope. *Rev. Sci. Instrum.* **1998**, *69*, 2072–2080.
20. Rost, M. J.; Crama, L.; Schakel, P.; van Tol, E.; van Velzen-Williams, G. B. E. M.; Overgauw, C. F.; ter Horst, H.; Dekker, H.; Okhuijsen, B.; Seynen, M.; *et al.* Scanning Probe Microscopes Go Video Rate and Beyond. *Rev. Sci. Instrum.* **2005**, *76*, 053710.
21. Delouise, L. A.; Winograd, N. Carbon-Monoxide Adsorption and Desorption on Rh(111) and Rh(331) Surfaces. *Surf. Sci.* **1984**, *138*, 417–431.